

## GAS ADSORPTION

# Multigas adsorption with single-site cooperativity in a metal–organic framework

Kurtis M. Carsch<sup>1,2</sup>, Henry Z. H. Jiang<sup>1,2,3</sup>, Ryan A. Klein<sup>4,5</sup>, Andrew S. Rosen<sup>3,6,7,8</sup>, Peyton S. Summerhill<sup>9</sup>, Jesse L. Peltier<sup>2,3</sup>, Adrian J. Huang<sup>1,2,3</sup>, Ryan A. Murphy<sup>2,3</sup>, Matthew N. Dods<sup>1,10</sup>, Hope A. Silva<sup>1,2</sup>, Zikri Hasanbasri<sup>11</sup>, Hyunchul Kwon<sup>1,2</sup>, Sarah L. Karstens<sup>1,2,3</sup>, Yuto Yabuuchi<sup>1,2,3</sup>, Jonas Börgel<sup>2,3</sup>, Jordan W. Taylor<sup>2</sup>, Katie R. Meihaus<sup>1,2</sup>, Karen C. Bustillo<sup>12</sup>, Andrew M. Minor<sup>7,12</sup>, Kristin A. Persson<sup>3,7</sup>, Craig M. Brown<sup>4,13</sup>, R. David Britt<sup>6,11</sup>, Nicholas P. Stadie<sup>9</sup>, Jeffrey R. Long<sup>1,2,3,7,10\*</sup>

Cooperative gas adsorption in metal–organic frameworks (MOFs) is a rare phenomenon that generally involves long-range communication between multiple binding sites. We demonstrate a MOF containing cobalt(II)–methyl sites that selectively and reversibly capture two carbon monoxide (CO) molecules per site, leading to record-high adsorption capacities at ambient temperatures and pressures. Gas adsorption and structural, spectroscopic, and computational analyses support a mechanism in which binding of one CO molecule triggers a spin transition, followed by binding of a second CO molecule and migratory insertion of the first CO molecule into the cobalt–methyl bond to form an acetyl. The greater binding affinity associated with the second CO results in sigmoidal adsorption isotherms, a hallmark of cooperativity and phase-change materials, despite the absence of long-range interactions within the framework.

Cooperativity, broadly defined as a set of molecular interactions in which the occurrence of a single event changes the free energies of other events (*1*), has been observed for gas binding in a small number of metal–organic frameworks (MOFs) (*2–6*). This phenomenon can lead to exceptional selectivities and high separation capacities, as observed for cooperative CO<sub>2</sub> uptake in polyamine-appended frameworks amine–Mg<sub>2</sub>(dobpdc) (dobpdc<sup>4−</sup> = 4,4′-dioxidobiphenyl-3,3′-dicarboxylate). At a threshold pressure in these materials, CO<sub>2</sub> inserts into the metal–amine bonds, triggering additional CO<sub>2</sub> binding events and the formation of ammonium carbamate chains running along one-dimensional (1D) channels within the framework (*5–9*). This mechanism is specific to CO<sub>2</sub>, and as a result, these materials exhibit high capacities for CO<sub>2</sub> even in the presence of other gases such as N<sub>2</sub>, O<sub>2</sub>, and water. The discovery of new mechanisms of gas binding in MOFs is an important driver of progress in the field of chemical separations with potentially far-reaching impacts, providing high working capacities with minimal pressure and temperature changes (*10–12*). However, materials exhibiting cooperative gas binding remain rare, and the only examples of cooperative adsorption discovered to

date involve communication between adjacent binding sites and long-range reorganization in at least one dimension.

Another phenomenon that is rare in MOFs is the binding of more than one gas molecule to a single metal site. Indeed, the metal sites in MOFs can generally only accommodate, at most, a single guest molecule, which inherently limits adsorption capacities. Among the thousands of MOF structures studied for gas adsorption to date, there are only three exceptions without long-range structural reorganization: Mn<sub>2</sub>(dsbdc) (dsbdc<sup>4−</sup> = 2,5-disulfido-1,4-benzenedicarboxylate), UTSA-74, an isomer of Zn<sub>2</sub>(dobdc) (dobdc<sup>4−</sup> = 2,5-dioxido-1,4-benzenedicarboxylate), and PCN-224-Co<sup>II</sup> (*13–15*). In the case of PCN-224-Co<sup>II</sup>, the noncooperative binding of two equivalents of CO per cobalt(II) site occurs only at very low temperatures, and noncooperative binding of two guest molecules in Mn<sub>2</sub>(dsbdc) and UTSA-74 is limited to a fraction of the available metal sites with suitable open coordination environments (*13, 14*).

Notably, an established mode of reactivity involving binding of two gas molecules at a single metal site has been reported for an organometallic complex. The reaction of two molecules of CO with pseudotetrahedral high-spin cobalt(II)–alkyl species yields a low-spin cobalt(II) monocarbonyl, monoacyl species (Fig. 1A) (*16–18*). The primary coordination sphere of the cobalt(II) ion in these molecules resembles that of the peripheral cobalt(II)–methyl sites in the framework material Co<sub>3.5</sub>Zn<sub>1.5</sub>(CH<sub>3</sub>)<sub>3.1</sub>Cl<sub>0.9</sub>(btdd)<sub>3</sub> [CoMe-MFU-4l; H<sub>2</sub>btdd = bis(*1H*-1,2,3-triazolo[4,5-*b*],[4′,5′-*z*])dibenzo[1,4]dioxin) (*19*), prepared through post-synthetic modification of MFU-4l [Zn<sub>5</sub>Cl<sub>4</sub>(btdd)<sub>3</sub>] (Fig. 1, B and C) (*20*).

We show that at ambient temperatures, CoMe-MFU-4l can reversibly and selectively capture two CO molecules per cobalt(II) site (Fig. 1D). In situ structural and spectroscopic analyses, in combination with density functional theory calculations, establish a mechanism of CO binding involving a high- to low-spin cobalt(II) spin state transition and tandem migratory insertion. Notably, the steep CO adsorption profile of this material could be well-modeled with either a sequential binding model, revealing a −6 kJ/mol cooperative binding energy, or a Hill–Langmuir model (*21*) with a Hill coefficient of  $n \approx 1.8$ , despite the adsorption occurring at individual cobalt(II) sites. This result highlights that long-range reorganization and communication between adjacent binding sites is not a prerequisite for adsorption to be steeper than that demonstrated for a Langmuir-type adsorbent. Both single-component adsorption data and breakthrough analysis revealed that this cooperative mechanism was highly selective for CO over other gases, including  $\pi$ -acids such as C<sub>2</sub>H<sub>4</sub>, even at very dilute CO concentrations.

## Synthesis and gas adsorption analysis

The framework CoMe-MFU-4l was previously synthesized from MFU-4l by exchange of the peripheral zinc(II) ions for cobalt(II) to yield Co<sub>4</sub>ZnCl<sub>4</sub>(btdd)<sub>3</sub>, or CoCl-MFU-4l (*22*), followed by anion metathesis with dimethylzinc [Zn(CH<sub>3</sub>)<sub>2</sub>] at ambient temperature to afford CoMe-MFU-4l [characterized as Co<sub>3.5</sub>Zn<sub>1.5</sub>(CH<sub>3</sub>)<sub>3.1</sub>Cl<sub>0.9</sub>(btdd)<sub>3</sub>] as a blue, air-sensitive powder (*19*). We found that starting with CoCl-MFU-4l, three sequential exchanges with excess Zn(CH<sub>3</sub>)<sub>2</sub> in tetrahydrofuran at 50°C resulted in a slightly greater extent of methylation, yielding a violet-blue powder with the chemical formula Co<sub>3.8</sub>Zn<sub>1.2</sub>(CH<sub>3</sub>)<sub>3.8</sub>Cl<sub>0.2</sub>(btdd)<sub>3</sub>, based on combustion analysis, inductively coupled plasma optical emission spectroscopy (ICP-OES), and energy-dispersive x-ray spectroscopy (EDX) [see supplementary materials (SM) section 6 for synthesis details and table S7]. Analysis of N<sub>2</sub> adsorption data obtained at 77 K for CoCl-MFU-4l and CoMe-MFU-4l revealed that both frameworks

<sup>1</sup>Baker Hughes Institute for Decarbonization Materials, University of California, Berkeley, Berkeley, CA, USA. <sup>2</sup>Department of Chemistry, University of California, Berkeley, Berkeley, CA, USA. <sup>3</sup>Materials Sciences Division, Lawrence Berkeley National Laboratory, Berkeley, CA, USA. <sup>4</sup>Center for Neutron Research, National Institute of Standards and Technology, Gaithersburg, MD, USA. <sup>5</sup>Material, Chemical, and Computational Sciences Directorate, National Renewable Energy Laboratory, Golden, CO, USA. <sup>6</sup>Miller Institute for Basic Research in Science, University of California, Berkeley, Berkeley, CA, USA. <sup>7</sup>Department of Materials Science and Engineering, University of California, Berkeley, Berkeley, CA, USA. <sup>8</sup>Department of Chemical and Biological Engineering, Princeton University, Princeton, NJ, USA. <sup>9</sup>Department of Chemistry and Biochemistry, Montana State University, Bozeman, MT, USA. <sup>10</sup>Department of Chemical and Biomolecular Engineering, University of California, Berkeley, Berkeley, CA, USA. <sup>11</sup>Department of Chemistry, University of California, Davis, Davis, CA, USA. <sup>12</sup>National Center for Electron Microscopy, Molecular Foundry, Lawrence Berkeley National Laboratory, Berkeley, CA, USA. <sup>13</sup>Chemical and Biomolecular Engineering, University of Delaware, Newark, DE, USA. \*Corresponding author. Email: jrlong@berkeley.edu

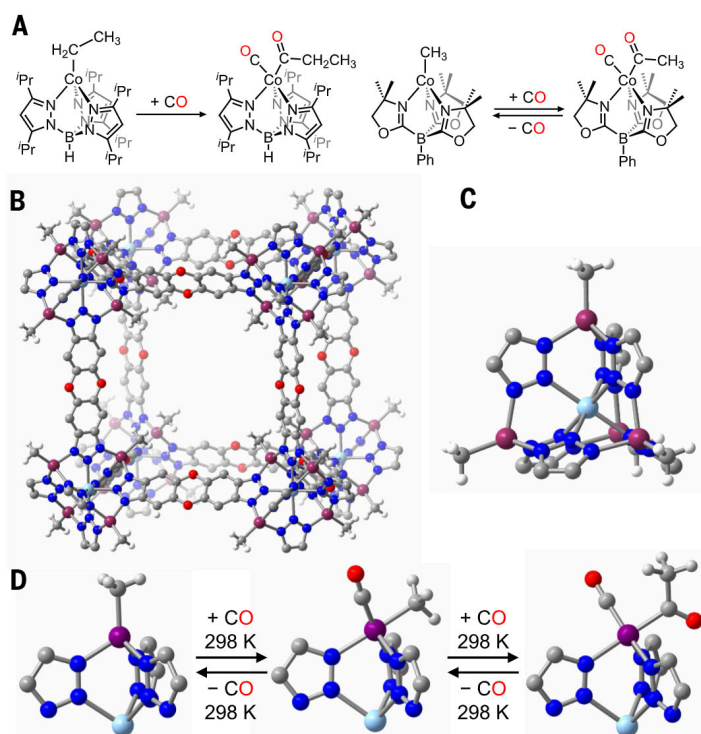


**Fig. 1. Design of a metal–organic framework for multiple binding of adsorbates at a single site.** (A) Literature precedent for carbonyl ligation and migratory insertion into pseudo-tetrahedral cobalt(II)-alkyl complexes (16–18). (B) A portion of the solid-state structure of CoMe-MFU-4l, as determined from single-crystal x-ray diffraction analysis (see SM section 8). (C) Depiction of the truncated pentanuclear CoMe-MFU-4l under various CO dosing conditions. The structures were determined from Rietveld refinements against synchrotron powder x-ray diffraction data for the starting and ending states (see SM section 7) with the intermediate geometry calculated using density functional theory (see SM section 10). Upon exposure to CO at ambient temperatures, CoMe-MFU-4l reversibly binds two equivalents of CO at its cobalt(II) sites to form a monocarbonyl, monoacetyl adduct. Light blue, purple, gray, blue, red, and white spheres represent Zn, Co, C, N, O, and H atoms, respectively. Hydrogen atoms on the linker are omitted for clarity.

were highly porous, with Brunauer–Emmett–Teller surface areas of 3800(40) and 3710(40)  $\text{m}^2/\text{g}$ , respectively (fig. S1). Single-crystal x-ray diffraction analysis of CoMe-MFU-4l (see SM section 8) showed the methyl ligand resided along a threefold symmetry axis with a Co–C<sub>Me</sub> bond length of 1.981(4) Å (fig. S39), consistent with Co–C<sub>Me</sub> distances reported for monoalkylated pseudo-tetrahedral high-spin cobalt(II) complexes (17, 23). Single-component CO adsorption and desorption isotherms were collected for CoCl-MFU-4l and CoMe-MFU-4l at 298 K and pressures up to 1 bar (see fig. S10 and Fig. 2A, respectively). Although CoCl-MFU-4l adsorbed very little CO under these conditions (~0.26 mmol/g at 1 bar), CoMe-MFU-4l exhibited a high affinity for CO at low partial pressures, adsorbing 5.18 mmol/g at just 10 mbar. This amount is much higher than expected if a single CO were to coordinate to each cobalt(II) site (3.1 to 3.3 mmol/g, see SM section 11 for details). At 1 bar, the CO capacity plateaued at a value of 6.07 mmol/g, near the expected value for binding of two CO molecules per cobalt(II) site.

Notably, the CO capacity achieved at 10 mbar and 298 K is the highest reported to date under these conditions for any MOF (24), and the 1 bar capacity is among the top few reported to date (table S12). Most other frameworks reported to date that exhibit high capacities for CO at ambient temperature feature open metal sites capable of binding just a single molecule of CO, for example Ni<sub>2</sub>(*m*-dobdc) (*m*-dobdc<sup>4-</sup> = 4,6-dioxido-1,3-benzenedicarboxylate; capacities of 3.8 and 5.7 mmol/g at 10 mbar and 1 bar, respectively) (25), although such sites have not been shown to be highly selective for CO over more polarizable gases such as C<sub>2</sub>H<sub>4</sub> (see fig. S18).

The high gravimetric CO capacity measured for CoMe-MFU-4l suggests a distinctive CO binding mechanism (discussed further below). Of note, single-component N<sub>2</sub>, H<sub>2</sub>, CH<sub>4</sub>, C<sub>2</sub>H<sub>6</sub>, and C<sub>2</sub>H<sub>4</sub> adsorption data collected for CoMe-MFU-4l and CoCl-MFU-4l at 298 K and pressures up to 1 bar were nearly identical, in contrast to the results for CO. For both frameworks, uptake of N<sub>2</sub>, H<sub>2</sub>, and CH<sub>4</sub> was <1 mmol/g at 1 bar, whereas uptake of C<sub>2</sub>H<sub>6</sub> and C<sub>2</sub>H<sub>4</sub> was slightly higher (~2.2 and ~2 mmol/g, respectively) (Fig. 2A and fig. S6). These data indicate that CoMe-MFU-4l and CoCl-MFU-4l exhibit similar mechanisms of gas adsorption for all these gases except for CO. As is common for metal-alkyl motifs, CoMe-MFU-4l is sensitive to O<sub>2</sub> in the presence or absence of CO. Although the products of dosing CoMe-MFU-4l with O<sub>2</sub> have not yet been identified, in situ diffuse reflectance infrared Fourier transform spectroscopy (DRIFTS) measurements on co-dosing CoMe-MFU-4l with O<sub>2</sub> and CO are consistent with formation of acetate within the framework, based on the new diagnostic vibrations at 1566 and 1435  $\text{cm}^{-1}$  (fig. S58). Finally, CO uptake in CoMe-MFU-4l was rapid (see figs. S14 to S16) and fully reversible as the adsorbed CO could be

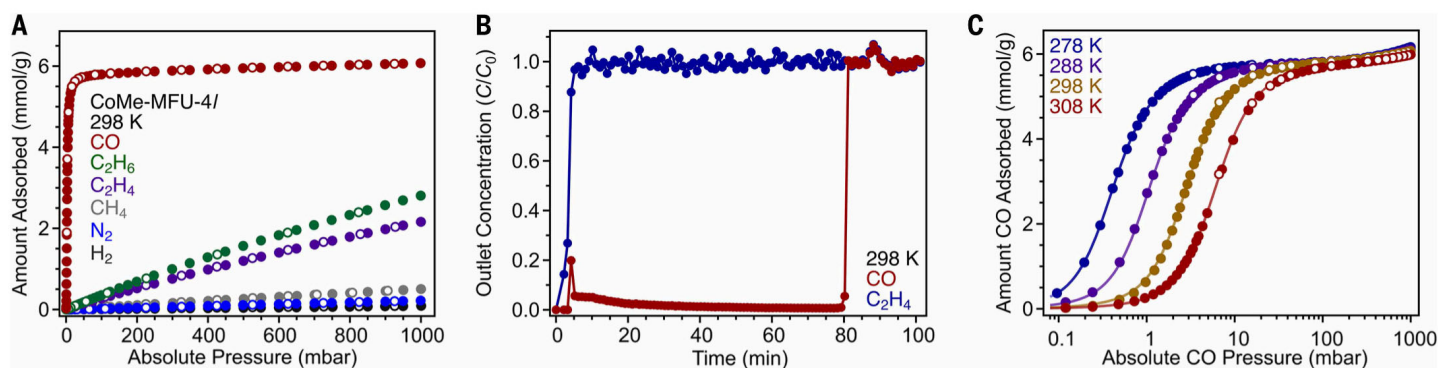


**Fig. 2. Gas adsorption studies of CoMe-MFU-4l.** (A) Single-component CO, C<sub>2</sub>H<sub>4</sub>, C<sub>2</sub>H<sub>6</sub>, CH<sub>4</sub>, N<sub>2</sub>, and H<sub>2</sub> adsorption and desorption isotherms obtained for CoMe-MFU-4l at 298 K. (B) Breakthrough data collected for a pelletized sample of CoMe-MFU-4l exposed to a flowing (10-sccm) gas stream consisting of 10% CO in C<sub>2</sub>H<sub>4</sub> at 298 K. See SM section 5 for details. (C) CO adsorption and desorption isotherms for CoMe-MFU-4l obtained at 278, 288, 298, and 308 K. Solid lines represent fits using the Hill equation with an additional Langmuir term (see SM section 3 and table S3 for details). From the fits, a Hill coefficient of  $n \approx 1.8$  was obtained.

## RESEARCH ARTICLES

desorbed under reduced pressure without hysteresis, and the framework retained more than 98% of its initial adsorption capacity after 50 isothermal adsorption (50 mbar CO in N<sub>2</sub>)/desorption (5 mbar CO in N<sub>2</sub>) cycles (fig. S12).

Analysis of the single-component gas adsorption data suggested that CoMe-MFU-4l should be highly selective for CO at dilute concentrations, even over other  $\pi$ -acids and more polarizable gases such as C<sub>2</sub>H<sub>4</sub>. To investigate this possibility, we conducted breakthrough analysis on a pelletized sample of CoMe-MFU-4l exposed to a flowing [10 standard cubic centimeters per minute (sccm)] stream containing 10% CO in C<sub>2</sub>H<sub>4</sub> at 298 K. After only 5 min, C<sub>2</sub>H<sub>4</sub> was detected at the outlet, corresponding to a capacity of 2.1 mmol/g (Fig. 2B), consistent with the C<sub>2</sub>H<sub>4</sub> capacity determined from single-component adsorption data at 900 mbar (2.0 mmol/g). Breakthrough of CO was detected after ~80 min, corresponding to a CO capacity of 5.9 mmol/g, again consistent with the capacity determined from single-component CO adsorption data at 100 mbar (5.8 mmol/g). These data indicate that the framework captured nearly two molecules of CO per cobalt(II) site even in the presence of C<sub>2</sub>H<sub>4</sub>. The similar capacities obtained from breakthrough analysis and single-component adsorption isotherms suggest that these two adsorbates do not compete for the same primary binding site, in contrast to the adsorption observed with frameworks such as Ni<sub>2</sub>(*m*-dobdc) (table S6).

### Modeling gas uptake in CoMe-MFU-4l

We could fit N<sub>2</sub>, H<sub>2</sub>, CH<sub>4</sub>, C<sub>2</sub>H<sub>6</sub>, and C<sub>2</sub>H<sub>4</sub> adsorption data collected for CoMe-MFU-4l over a range of temperatures using a single-site (N<sub>2</sub>, CH<sub>4</sub>, C<sub>2</sub>H<sub>6</sub>, and C<sub>2</sub>H<sub>4</sub>) or dual-site (H<sub>2</sub>) Langmuir–Freundlich model. The resulting fit parameters were used with the Clausius–Clapeyron relation to estimate isosteric enthalpies of adsorption ( $\Delta H_{\text{ads}}$ ) ranging from  $-7$  to  $-20$  kJ/mol, within the range of values expected for physisorption of these gases (fig. S10 and table S4) (26). By contrast, application of a single-site Langmuir model to the low-pressure CO adsorption data for CoMe-MFU-4l provided an unsatisfactory fit (fig. S40).

Considering the sharp CO uptake in CoMe-MFU-4l and the evidence of multiple guests binding to a single cobalt(II) site, we considered instead that CO binding at the cobalt(II) sites may be occurring in a fashion where binding of one equivalent of CO facilitated a second binding event at the same site. Although mechanistically distinct, cooperative gas uptake in diamine-appended Mg<sub>2</sub>(dobpdc) and related diamine–Mg<sub>2</sub>(olz) materials [olz<sup>4-</sup> = (*E*)-5,5'-(diazene-1,2-diyl)bis(2-oxidobenzoate)] (27) has been qualitatively modeled using a version of the Hill equation (21) adapted for fitting adsorption data. From these fits, the Hill coefficient  $n$  could be extracted, in which  $n > 1$  is indicative of positive cooperativity (28–30). For diamine–Mg<sub>2</sub>(dobpdc) and diamine–Mg<sub>2</sub>(olz), values of  $n$  are typically  $\geq 3$  and have been used for comparison of the degree of cooperativity in CO<sub>2</sub> uptake in these materials, with  $n$  qualitatively interpreted to indicate the average number of CO<sub>2</sub> molecules required for adsorption to occur (5, 27).

In the case of CoMe-MFU-4l, the CO adsorption data obtained for CoMe-MFU-4l at 278, 288, 298, and 308 K (Fig. 2C and table S5; see SM section 1.4) could be well fit with a sequential binding model (see SM section 3 for statistical mechanics derivation), revealing a cooperative binding energy of  $-6$  kJ/mol, reflecting a stronger binding of the second CO to the cobalt site relative to that of the first CO. Notably, single- or double-site Langmuir models appropriate for describing strong and distinct metal–adsorbate interactions failed to adequately model the

adsorption profile. These data could be modeled by including a Hill parameter to describe the strong binding site (see SM section 3 for details). This yields a Hill coefficient of  $n = 1.8$  and a saturation capacity of 5.70 mmol/g, consistent with cooperative uptake of two molecules of CO at each cobalt(II) site (fig. S9 and table S3) (30). Although the data could be accurately fit with either sequential or Hill models, we favor the sequential binding model as it reflects the underlying reaction progression as ascertained from spectroscopic data (see below). The fit parameters obtained from fitting the full 298 K isotherm for CoMe-MFU-4l were then used with the Clausius–Clapeyron relation to calculate  $\Delta H_{\text{ads}}$  as a function of CO loading, revealing a relatively constant  $\Delta H_{\text{ads}}$  of approximately  $-64$  kJ/mol per CO (table S4). The magnitude of the CO binding enthalpy in this case is much greater than reported for most other MOFs (25, 31) and comparable to the enthalpy of CO adsorption reported for Fe<sub>2</sub>Cl<sub>2</sub>(bbta) ( $\Delta H_{\text{ads}} = -65$  kJ/mol), which captures one molecule of CO per iron(II) site through a cooperative spin transition mechanism (3, 24). Although the air sensitivity of CoMe-MFU-4l may still need to be addressed for some CO separations, it could be of immediate service for a number of potential applications, including purity augmentation for prepurified streams, CO scavenging from H<sub>2</sub> streams for ammonia production and fuel cell technologies, and last-step purification of gas streams in catalysis applications (32).

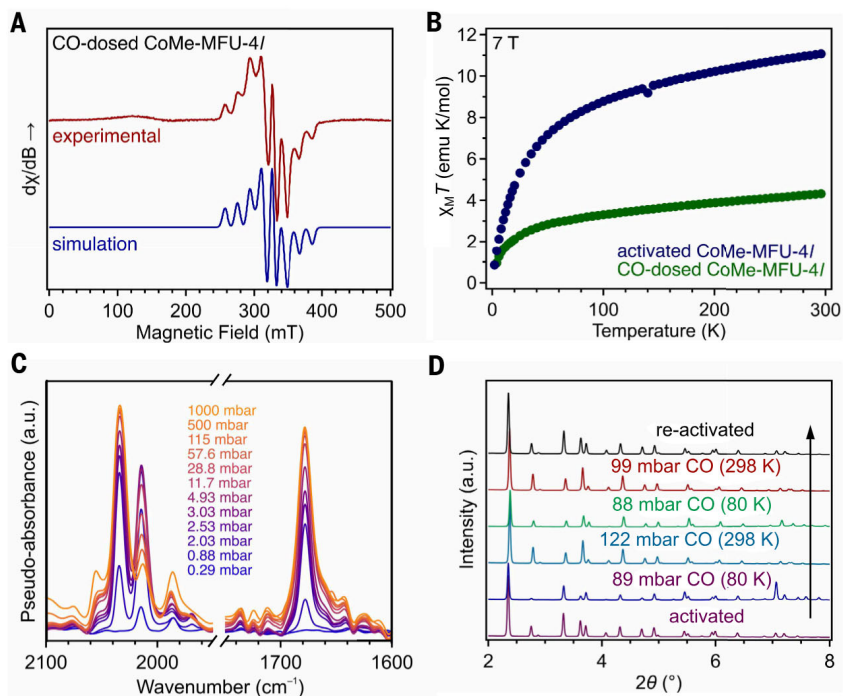


**Fig. 3. Spectroscopic and structural characterization of reversible CO uptake in CoMe-MFU-4l.** (A) X-band electron paramagnetic resonance spectrum (red trace, collected at 15 K) for a sample of cobalt-dilute CoMe-MFU-4l dosed with 50 mbar of CO at 298 K. A simulated spectrum using the software EasySpin (see SM section 1.13 for details). Fitting parameters are  $g_x = 2.076$ ,  $g_y = 2.041$ ,  $g_z = 2.081$ ,  $A_x = 120$  MHz,  $A_y = 120$  MHz, and  $A_z = 535$  MHz. (B) Temperature dependence of the molar magnetic susceptibility–temperature product ( $\chi_M T$ ) for activated CoMe-MFU-4l and a sample of CoMe-MFU-4l dosed with 500 mbar CO. The lower magnitude of  $\chi_M T$  across the entire temperature range upon CO dosing is consistent with a transition from high- to low-spin cobalt(II) upon CO binding. (C) Difference spectra generated by subtracting evolving spectra collected for CO-dosed CoMe-MFU-4l from the spectrum of CoMe-MFU-4l at 298 K. The data revealed the growth of several new vibrations, including a prominent acetyl vibrational band at 1678 cm<sup>-1</sup> that appears concomitant with a peak for a red-shifted CO. (D) Representative synchrotron powder x-ray diffraction patterns collected over the course of the in situ gas dosing experiment (see SM section 7 for details and figs. S31 to S33 for the full set of data). At 80 K, CO only physisorbed within the material whereas upon dosing with ~100 mbar at 298 K, migratory insertion and coordination of CO to the cobalt(II) ions was observed. Select patterns are shown to highlight changes with heating under the different gas atmospheres. a.u., arbitrary units

## Mechanism of CO adsorption

Upon exposure to 1 bar of CO, CoMe-MFU-4l rapidly changed from violet to light brown, whereas subsequent exposure to vacuum reversed this color change, suggesting a reversible electronic structure change at the cobalt center that occurred upon CO binding (fig. S39). Analysis on a cobalt-dilute sample of CoMe-MFU-4l with solid-state electron paramagnetic resonance (EPR) spectroscopy at 15 K revealed an eight-line hyperfine splitting pattern consistent with a high-spin cobalt(II) center (nuclear spin  $I_{\text{Co}} = 7/2$ , fig. S23). By contrast, the EPR spectrum obtained for a sample of CoMe-MFU-4l dosed *ex situ* with 50 mbar of CO featured a prominent eight-line pattern between 240 and 400 mT ( $g \approx 2.0$  and 2.1), consistent with a low-spin cobalt(II) center, along with a very low-intensity  $S = 3/2$  signal (Fig. 3A).

Direct current magnetic susceptibility data collected for CoMe-MFU-4l and a sample of CoMe-MFU-4l dosed with 500 mbar of CO also support a cobalt(II) spin state change upon CO adsorption (Fig. 3B). At 300 K and 7 T, the product of the experimental molar magnetic susceptibility and temperature ( $\chi_{\text{M}}T$ ) determined for CoMe-MFU-4l was 11.1 electromagnetic units (emu) K mol<sup>-1</sup>. In contrast, at 300 K and 7 T, the magnitude of  $\chi_{\text{M}}T$  for the CO-dosed sample of CoMe-MFU-4l was much lower at 4.3 emu K mol<sup>-1</sup>. The magnitude of  $\chi_{\text{M}}T$  for both samples was higher than the predicted magnitude for four isotropic  $S = 3/2$  or  $1/2$  cobalt(II) centers, respectively (7.5 and 1.50 emu K mol<sup>-1</sup> per formal unit), which can be attributed to the presence of magnetic anisotropy, whereas the much smaller  $\chi_{\text{M}}T$  magnitude for the CO-dosed sample was consistent with a change from high-spin to low-spin cobalt(II) upon CO binding (see SM section 5.3 for further discussion).

To monitor chemical changes occurring upon CO binding, *in situ* variable-pressure and variable-temperature DRIFTS data were obtained upon dosing samples of CoMe-MFU-4l with various pressures of CO and <sup>13</sup>CO (up to 1 bar, see fig. S28 for the isotopically labeled spectrum). To eliminate any effects arising from electronic communication between cobalt(II) sites in the same cluster node, we synthesized a variant of CoMe-MFU-4l with an average ratio of 1.0:4.0 Co:Zn based on ICP-OES, consistent with presence of just one cobalt per cluster node on average (33). We collected difference spectra upon dosing with increasing pressures of CO at 300 K, with the activated framework as the baseline. Corresponding spectra for undiluted CoMe-MFU-4l appeared similar, with broader features (see fig. S24). This procedure resulted in complex spectra with multiple peaks and overlapping vibrational bands.

Four main CO-based vibrations at 2034, 2015, 1986, and 1678 cm<sup>-1</sup> (Fig. 3C) were observed. At low pressures, the vibrational band at 1986 cm<sup>-1</sup> saturated quickly at mbar pressure and persisted even after exposing the sample to dynamic vacuum. While we cannot discount  $\nu(\text{C}\equiv\text{O})$  vibrations due to CO ligation at defect sites, this  $\nu(\text{C}\equiv\text{O})$  value resembles that of monocarbonyl cobalt(I) complexes (34), potentially located at surface sites and generated from reduction induced by the methyl anion (3) (see fig. S25 and table S8). The 2015 cm<sup>-1</sup> peak initially increased with increasing CO pressures up to ~5 mbar and then decreased in intensity at higher pressures up to 1 bar, thus we assigned this band as  $\nu(\text{C}\equiv\text{O})$  for a single CO bound at the cobalt site, yielding a monocarbonyl, monomethyl cobalt(II) complex.

Above ~0.3 mbar, two other bands appeared at 1678 and 2034 cm<sup>-1</sup> and increased in intensity throughout the experiment up to 1 bar. We assigned these features to a cobalt-acetyl (18) and a monocarbonyl, monoacetyl cobalt (II) complex, respectively. The  $\nu(\text{C}\equiv\text{O})$  of the CO on the cobalt-acetyl complex is hypsochromically shifted when compared to the  $\nu(\text{C}\equiv\text{O})$  of the CO on the cobalt-methyl complex, consistent with observations for molecular analogs in solution (18). Furthermore, variable-temperature studies indicated that neither the monocarbonyl, monoalkyl complex, nor the monocarbonyl, monoacetyl cobalt(II) complex form when the material was directly dosed with CO at 100 K. However, if the material was dosed at 300 K and then cooled, these

products persist, indicating activation barriers for their formation (figs. S26 and S27).

*In situ* powder x-ray diffraction data were collected for a sample of CoMe-MFU-4l dosed with CO to examine structural changes occurring as a function of temperature (see Fig. 3D and section 7.2 of the SM). Starting from a sample of activated CoMe-MFU-4l at 80 K, dosing with increasing pressures of CO ranging from 12 to 89 mbar resulted in clear changes in the diffraction patterns, for example, a decrease in the intensity of peaks at  $2\theta = 2.75^\circ$ ,  $3.88^\circ$ , and  $4.07^\circ$  and an increase in the intensity of the peak at  $7.15^\circ$  (fig. S29A).

A Rietveld refinement of the diffraction pattern obtained after dosing with 12 mbar of CO revealed physisorbed CO within the framework (fig. S35, consistent with DRIFTS data collected at 100 K; see fig. S25). Heating the sample from 80 to 298 K after dosing with 89 mbar of CO resulted in a large unit-cell contraction that was complete at around 150 K, which was consistent with a transition from high- to low-spin cobalt(II) (fig. S32) and consistent with the EPR spectroscopy and magnetic susceptibility data.

After subsequent cooling from 298 K under 89 mbar CO and then heating to 313 K under a vacuum to regenerate the sample, powder x-ray diffraction data were collected at 298 K under increasing pressures of CO from 11 to 99 mbar. Changes in the diffraction data were again consistent with a unit-cell contraction and a conversion from high- to low-spin cobalt(II), and Rietveld refinement of the diffraction pattern collected at 99 mbar supported the presence of a monocarbonyl, monoacetyl adduct of cobalt(II), consistent with the features observed in the vibrational spectra (figs. S36 and S37). Finally, heating at 313 K under a dynamic vacuum regenerated the diffraction pattern for CoMe-MFU-4l, illustrating the reversibility of CO coordination and migratory insertion (fig. S37).

To further investigate the mechanism of CO adsorption in CoMe-MFU-4l, density functional theory (DFT) calculations were performed with  $\text{Co}_4\text{Zn}(\text{CH}_3)_4(\text{bta})_6$  ( $\text{bta}^- = \text{benzotriazolate}$ ) as a representative cluster model (Fig. 4; see SM section 10 for details). Key vibrations from DRIFTS measurements could be recapitulated in models with sorption confined to a single cobalt(II) site (table S9). A summary of the most important mechanistic steps is shown in Fig. 4, with additional details provided in figs. S47 to S55 and tables S14 to S30. The

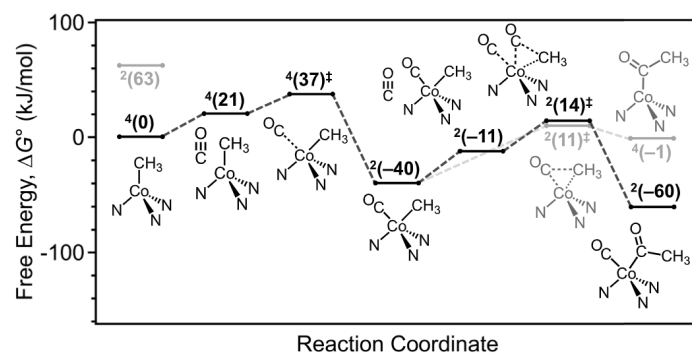


**Fig. 4. Calculated free energy landscape for reversible CO coordination and migratory insertion into the Co-Me bond.** Standard-state free energy landscape (kJ/mol) at 298.15 K and 1 atm using the M06-L/def2-TZVP level of theory for the reaction of CO with the model cluster  $\text{Co}_4\text{Zn}(\text{CH}_3)_4(\text{bta})_6$  at a single cobalt(II) site with initial ligation and spin-transition to yield  $\text{Co}_4\text{Zn}(\text{CH}_3)_4(\text{CO})(\text{bta})_6$ , followed by coordination and migratory insertion of the second equivalent of CO to yield  $\text{Co}_4\text{Zn}(\text{CH}_3)_3(\text{CO})(\text{COMe})(\text{bta})_6$ . The superscript preceding the energy values denotes the spin multiplicity ( $2S+1$ ) for the Co site to which CO binding is analyzed. Alternative mechanistic pathways, including direct migratory insertion from  $\text{Co}_4\text{Zn}(\text{CH}_3)_4(\text{CO})(\text{bta})_6$  and the coordination of two CO equivalents to the same cobalt site, as depicted in gray, are both thermodynamically and kinetically less favorable. See SM section 10 for computational details.

## RESEARCH ARTICLES

most energetically favorable series of elementary steps begins with the adsorption of CO to a high-spin cobalt site, resulting in a spin transition from  $S = 3/2$  to  $S = 1/2$  at the cobalt ion and a corresponding change in coordination geometry from tetrahedral to distorted trigonal bipyramidal. Notably, the DFT calculations suggest that CO binding at one cobalt(II) site does not greatly alter the energetic landscape for CO adsorption elsewhere in the cluster (tables S16 and S18).

After the CO-induced spin transition, a second CO molecule is predicted to adsorb at the same cobalt(II) center, in which chemisorption of the second CO molecule occurs with a concomitant migratory insertion of the first CO adsorbate into the terminal methyl ligand, yielding a monocarbonyl, monoacetyl group (figs. S53 and S55). The concerted adsorption–reaction step, which takes place along the low-spin surface, is predicted to be critical to the adsorption capability of CoMe-MFU-4l for multiple equivalents of CO. Alternative reaction pathways, including formation of a dicarbonyl intermediate or direct migratory insertion of the first CO to yield a monoacetyl intermediate were calculated as higher energy pathways (Fig. 4).

## Outlook

The foregoing results demonstrate that the highly porous metal-organic framework CoMe-MFU-4l selectively and reversibly captures two equivalents of CO per cobalt(II)-methyl site through a tandem spin transition and reversible migratory insertion mechanism. This process resulted in highly selective, high-capacity CO capture with a dependence on substrate that rendered the adsorption profile akin to that of other cooperative adsorbents without the need for long-range structural reorganization. More broadly, this work raises the prospect of judiciously designing porous adsorbents with adsorption sites that can bind multiple guest molecules.

## REFERENCES AND NOTES

1. A. Whitty, *Nat. Chem. Biol.* **4**, 435–439 (2008).
2. C. M. McGuirk *et al.*, *Nat. Commun.* **9**, 5133 (2018).
3. D. A. Reed *et al.*, *Nature* **550**, 96–100 (2017).
4. J. Oktawiec *et al.*, *Nat. Commun.* **11**, 3087 (2020).
5. T. M. McDonald *et al.*, *Nature* **519**, 303–308 (2015).
6. E. J. Kim *et al.*, *Science* **369**, 392–396 (2020).
7. R. L. Siegelman *et al.*, *J. Am. Chem. Soc.* **139**, 10526–10538 (2017).
8. J. R. Edison *et al.*, *J. Chem. Phys.* **154**, 214704 (2021).
9. J. Kundu *et al.*, *Phys. Rev. Lett.* **121**, 015701 (2018).
10. B. E. R. Snyder *et al.*, *Nature* **613**, 287–291 (2023).
11. R. C. Rohde *et al.*, *Science* **386**, 814–819 (2024).
12. A. M. Wright, M. T. Kapelewski, S. Marx, O. K. Farha, W. Morris, *Nat. Mater.* **24**, 178–187 (2025).
13. F. Luo *et al.*, *J. Am. Chem. Soc.* **138**, 5678–5684 (2016).
14. T. Runčevski *et al.*, *Chem. Commun.* **52**, 8251–8254 (2016).
15. A. T. Gallagher, C. D. Malliakas, T. D. Harris, *Inorg. Chem.* **56**, 4654–4662 (2017).
16. N. Shirasawa, M. Akita, S. Hikichi, Y. Moro-oka, *Chem. Commun.* **5**, 417–418 (1999).
17. R. R. Reinig, E. L. Fought, A. Ellern, T. L. Windus, A. D. Sadow, *Chem. Commun.* **53**, 11020–11023 (2017).
18. R. R. Reinig, E. L. Fought, A. Ellern, T. L. Windus, A. D. Sadow, *Dalton Trans.* **47**, 12147–12161 (2018).
19. R. Röb-Ohlenroth, B. Bredenkötter, D. Volkmer, *Organometallics* **38**, 3444–3452 (2019).
20. D. Denysenko *et al.*, *Chemistry* **17**, 1837–1848 (2011).
21. R. Gesztelyi *et al.*, *Arch. Hist. Exact Sci.* **66**, 427–438 (2012).
22. D. Denysenko *et al.*, *Chem. Commun.* **48**, 1236–1238 (2012).
23. J. D. Jewson, L. M. Liable-Sands, G. P. A. Yap, A. L. Rheingold, K. H. Theopold, *Organometallics* **18**, 300–305 (1999).
24. X. Ma *et al.*, *Chem. Soc. Rev.* **52**, 3741–3777 (2023).
25. J. E. Bachman *et al.*, *Energy Environ. Sci.* **11**, 2423–2431 (2018).
26. D. Farrusseng *et al.*, *Langmuir* **25**, 7383–7388 (2009).
27. Z. Zhu *et al.*, *J. Am. Chem. Soc.* **145**, 17151–17163 (2023).
28. J. N. Weiss, *FASEB J.* **11**, 835–841 (1997).
29. A. V. Hill, *Biochem. J.* **7**, 471–480 (1913).
30. H. Swenson, N. P. Stadie, *Langmuir* **35**, 5409–5426 (2019).
31. E. D. Bloch *et al.*, *J. Am. Chem. Soc.* **136**, 10752–10761 (2014).
32. J. J. Baschuk, X. Li, *Int. J. Energy Res.* **25**, 695–713 (2001).

33. A. M. Wright, A. J. Rieth, S. Yang, E. N. Wang, M. Dincă, *Chem. Sci.* **9**, 3856–3859 (2018).
34. D. Denysenko, J. Jelic, K. Reuter, D. Volkmer, *Chemistry* **21**, 8188–8199 (2015).

## ACKNOWLEDGMENTS

We thank H. Celik, R. Giovine, and the Pines Magnetic Resonance Center's Core NMR Facility (PMRC Core) for assistance with spectroscopic measurements and analyses. The instrument used in this work was supported by the National Science Foundation under grant 2018784. Powder x-ray diffraction data were collected at Beamline 17-BM-B at the Advanced Photon Source, a US Department of Energy (DOE) Office of Science User Facility, operated by Argonne National Laboratory under contract DE-AC02-06CH11357. We thank A. Yakovenko (Argonne National Laboratory) for technical assistance with powder x-ray diffraction data refinement, L. M. Mirica (University of Illinois Urbana-Champaign) for helpful discussions on cooperativity, T. D. Harris (University of California, Berkeley) for editorial assistance, and D. X. Ngo, R. C. Rohde, and B. E. R. Snyder (University of California, Berkeley) for general discussions. **Funding:** Gas adsorption analyses, crystal structure determinations, spectroscopic measurements, and electronic structure calculations were supported by the DOE, Office of Basic Energy Sciences (BES), Separation Science in the Chemical Sciences, Geosciences, and Biosciences Division, under award number DE-SC0019992. The synthesis of materials was supported by the Hydrogen Materials–Advanced Research Consortium (HyMARC), established as part of the Energy Materials Network under the DOE, Office of Energy Efficiency and Renewable Energy, Hydrogen and Fuel Cell Technologies Office, under contract DE-AC02-05CH11231. K.M.C. was supported by an Arnold O. Beckman Postdoctoral Fellowship, J.L.P. acknowledges support from both the University of California President's and the Ford Foundation Postdoctoral Fellowship Programs, A.S.R. acknowledges support via a Miller Research Fellowship from the Miller Institute for Basic Research in Science at the University of California, Berkeley, and J.B. acknowledges the Deutsche Forschungsgemeinschaft (DFG) for a postdoctoral research fellowship. Magnetic measurements were supported by National Science Foundation (NSF) grant DMR-2206534. R.A.M. was supported in part through the Quantum Information Science and Engineering Network (NSF grant DMR-1747426). This research used the Savio computational cluster resource provided by the Berkeley Research Computing program at the University of California, Berkeley (supported by the UC Berkeley Chancellor, Vice Chancellor for Research, and Chief Information Officer). R.D.B. acknowledges National Institutes of Health (NIH) Grant R35-GM126961 for EPR instrumentation and measurements. R.A.K. acknowledges the DOE Office of Energy Efficiency and Renewable Energy (EERE), Hydrogen and Fuel Cell Technologies Office (HFTO) contract no. DE-AC36-8G028308 to the National Renewable Energy Laboratory (NREL). Electron microscopy was supported by the DOE, Office of Science, BES, Materials Sciences and Engineering Division under contract DE-AC02-05-CH11231 within the Electron Microscopy of Soft Matter Program (KC11BN) and carried out at the Molecular Foundry, which is supported by the Office of Science, Office of Basic Energy Sciences, of the DOE under contract DE-AC02-05CH11231. P.S.S. and N.P.S. acknowledge funding from NSF grant CHE-2349748. Work at the Molecular Foundry was supported by the Office of Science, Office of BES, of the DOE under contract DE-AC02-05CH11231. Certain commercial equipment, instruments, or materials are identified in this document. Such identification does not imply recommendation or endorsement by the National Institute of Standards and Technology (NIST), nor does it imply that the products identified are necessarily the best available for the purpose. C.M.B. was fully supported and R.A.K. was partially supported by NIST during this project. The views expressed in the article do not necessarily represent the views of the DOE or the US Government. The US Government retains and the publisher, by accepting the article for publication, acknowledges that the US Government retains a nonexclusive, paid-up, irrevocable, worldwide license to publish or reproduce the published form of this work, or allow others to do so, for US Government purposes. **Author contributions:** K.M.C., J.B., and J.R.L. conceptualized the research. K.M.C. synthesized and characterized materials, directed the research with J.R.L., and analyzed data. J.L.P. and A.J.H. conducted and interpreted breakthrough analyses. H.Z.H.J., S.H.K., K.M.C., J.L.P., H.A.S., Y.Y., Z.K., R.D.B., and J.B. conducted spectroscopic characterization. R.A.M. conducted and interpreted magnetometry. K.M.C., M.D., and Y.Y. conducted gas adsorption isotherm measurements. K.M.C., J.L.P., H.K., and J.W.T. performed single-crystal x-ray diffraction analyses. R.A.K. and C.M.B. collected and analyzed powder x-ray diffraction data. P.S.S. and N.P.S. developed the sequential binding model for the CO adsorption data. A.S.R. and K.A.P. performed computational analyses. K.M.C. and K.R.M. drafted the manuscript. All authors contributed to revision of the manuscript. **Competing interests:** The authors declare the following competing interests: The University of California, Berkeley, has applied for a patent on some of the technology discussed herein regarding gas separations with coordinatively unsaturated metal carbanions, on which K.M.C., J.L.P., J.B., and J.R.L. are listed as coinventors. **Data and materials availability:** The supplementary materials contain complete experimental and spectral details for all new compounds reported herein. Crystallographic data for solid-state structures obtained from single-crystal x-ray diffraction have been made available free of charge from the Cambridge Crystallographic Data Centre (CCDC) under deposition number 2352633 for CoMe-MFU-4l. **License information:** Copyright © 2025 the authors, some rights reserved; exclusive licensee American Association for the Advancement of Science. No claim to original US government works. <https://www.science.org/content/page/science-licenses-journal-article-reuse>

## SUPPLEMENTARY MATERIALS

[science.org/doi/10.1126/science.ady2607](https://science.org/doi/10.1126/science.ady2607)

Materials and Methods; Figs. S1 to S59; Tables S1 to S30; Technical discussions on magnetometry, powder x-ray diffraction, anion stoichiometry, small molecule reactivity, and sequential binding model; Supplemental adsorption information format (AIF) files; References (35–84)

Submitted 15 April 2025; accepted 23 September 2025

10.1126/science.ady2607